Search for point sources of high energy neutrinos with final data from AMANDA-II

R. Abbasi,[23] M. Ackermann,[35] J. Adams,[13] M. Ahlers,[27] J. Ahrens,[24] K. Andeen,[23] J. Auffenberg,[34] X. Bai,[26] M. Baker,[23] B. Baret,[11] S. W. Barwick,[19] R. Bay,[7] J. L. Bazo Alba,[35] K. Beattie,[8] T. Becka,[24] J. K. Becker,[16] K.-H. Becker,[34] J. Berdermann,[35] P. Berghaus,[23] D. Berley,[14] E. Bernardini,[35] D. Bertrand,[10] D. Z. Besson,[21] E. Blaufuss,[14] D. J. Boersma,[23] C. Bohm,[29] J. Bolmont,[35] S. Böser,[35] O. Botner,[32] J. Braun,[23,*] D. Breder,[34] T. Burgess,[29] T. Castermans,[25] D. Chirkin,[23] B. Christy,[14] J. Clem,[26] D. F. Cowen,[31,30] M. V. D'Agostino,[7] M. Danninger,[13] A. Davour,[32] C. T. Day,[8] O. Depaepe,[11] C. De Clercq,[11] L. Demirörs,[20] F. Descamps,[17] P. Desiati,[23] G. de Vries-Uiterweerd,[17] T. DeYoung,[31] J. C. Diaz-Velez,[23] J. Dreyer,[16] J. P. Dumm,[23] M. R. Duvoort,[33] W. R. Edwards,[8] R. Ehrlich,[14] J. Eisch,[23] R. W. Ellsworth,[14] O. Engdegård,[32] S. Euler,[1] P. A. Evenson,[26] O. Fadiran,[4] A. R. Fazely,[6] K. Filimonov,[7] C. Finley,[23] M. M. Foerster,[31] B. D. Fox,[31] A. Franckowiak,[9] R. Franke,[35] T. K. Gaisser,[26] J. Gallagher,[22] R. Ganugapati,[23] L. Gerhardt,[8,7] L. Gladstone,[23] A. Goldschmidt,[8] J. A. Goodman,[14] R. Gozzini,[24] D. Grant,[31] T. Griesel,[24] A. Groß,[13,18] S. Grullon,[23] R. M. Gunasingha,[6] M. Gurtner,[34] C. Ha,[31] A. Hallgren,[32] F. Halzen,[23] K. Han,[13] K. Hanson,[23] R. Hardtke,[28] Y. Hasegawa,[12] J. Heise,[33] K. Helbing,[34] M. Hellwig,[24] P. Herquet,[25] S. Hickford,[13] G. C. Hill,[23] J. Hodges,[23] K. D. Hoffman,[14] K. Hoshina,[23] D. Hubert,[11] W. Huelsnitz,[14] B. Hughey,[23] J.-P. Hülß,[1] P. O. Hulth,[29] K. Hultqvist,[29] S. Hundertmark,[29] S. Hussain,[26] R. L. Imlay,[6] M. Inaba,[12] A. Ishihara,[12] J. Jacobsen,[23] G. S. Japaridze,[4] H. Johansson,[29] J. M. Joseph,[8] K.-H. Kampert,[34] A. Kappes,[23,†] T. Karg,[34] A. Karle,[23] H. Kawai,[12] J. L. Kelley,[23] J. Kiryluk,[8,7] F. Kislat,[35] S. R. Klein,[8,7] S. Klepser,[35] G. Kohnen,[25] H. Kolanoski,[9] L. Köpke,[24] M. Kowalski,[9] T. Kowarik,[24] M. Krasberg,[23] K. Kuehn,[15] T. Kuwabara,[26] M. Labare,[10] K. Laihem,[1] H. Landsman,[23] R. Lauer,[35] H. Leich,[35] D. Leier,[16] C. Lewis,[23] A. Lucke,[9] J. Lundberg,[32] J. Lünemann,[24] J. Madsen,[28] R. Maruyama,[23] K. Mase,[12] H. S. Matis,[8] C. P. McParland,[8] K. Meagher,[14] A. Meli,[16] M. Merck,[23] T. Messarius,[16] P. Mészáros,[31,30] H. Miyamoto,[12] A. Mohr,[9] T. Montaruli,[23,‡] R. Morse,[23] S. M. Movit,[30] K. Münich,[16] R. Nahnhauer,[35] J. W. Nam,[19] P. Nießen,[26] D. R. Nygren,[8,29] S. Odrowski,[18] A. Olivas,[14] M. Olivo,[32] M. Ono,[12] S. Panknin,[9] S. Patton,[8] C. Pérez de los Heros,[32] J. Petrovic,[10] A. Piegsa,[24] D. Pieloth,[35] A. C. Pohl,[32,§] R. Porrata,[7] N. Potthoff,[34] J. Pretz,[14] P. B. Price,[7] G. T. Przybylski,[8] K. Rawlins,[3] S. Razzaque,[31,30] P. Redl,[14] E. Resconi,[18] W. Rhode,[16] M. Ribordy,[20] A. Rizzo,[11] W. J. Robbins,[31] J. Rodriguez,[23] P. Roth,[14] F. Rothmaier,[24] C. Rott,[15] C. Roucelle,[18] D. Rutledge,[31] D. Ryckbosch,[17] H.-G. Sander,[24] S. Sarkar,[27] K. Satalecka,[35] S. Schlenstedt,[35] T. Schmidt,[14] D. Schneider,[23] O. Schultz,[18] D. Seckel,[26] B. Semburg,[34] S. H. Seo,[29] Y. Sestayo,[18] S. Seunarine,[13] A. Silvestri,[19] A. J. Smith,[14] C. Song,[23] G. M. Spiczak,[28] C. Spiering,[35] M. Stamatikos,[15] T. Stanev,[26] T. Stezelberger,[8] R. G. Stokstad,[8] M. C. Stoufer,[8] S. Stoyanov,[26] E. A. Strahler,[23] T. Straszheim,[14] K.-H. Sulanke,[35] G. W. Sullivan,[14] Q. Swillens,[10] I. Taboada,[5] O. Tarasova,[35] A. Tepe,[34] S. Ter-Antonyan,[6] S. Tilav,[26] M. Tluczykont,[35] P. A. Toale,[31] D. Tosi,[35] D. Turčan,[14] N. van Eijndhoven,[33] J. Vandenbroucke,[7] A. Van Overloop,[17] V. Viscomi,[31] C. Vogt,[1] B. Voigt,[35] C. Walck,[29] T. Waldenmaier,[9] M. Walter,[35] C. Wendt,[23] S. Westerhoff,[23] N. Whitehorn,[23] C. H. Wiebusch,[1] C. Wiedemann,[16] G. Wikström,[29] D. R. Williams,[2] R. Wischnewski,[35] H. Wissing,[1,14] K. Woschnagg,[7] X. W. Xu,[6] G. Yodh,[19] and S. Yoshida[12]

(IceCube Collaboration)

[1]*III Physikalisches Institut, RWTH Aachen University, D-52056 Aachen, Germany*
[2]*Department of Physics and Astronomy, University of Alabama, Tuscaloosa, Alabama 35487, USA*
[3]*Department of Physics and Astronomy, University of Alaska Anchorage, 3211 Providence Drive, Anchorage, Alaska 99508, USA*
[4]*CTSPS, Clark-Atlanta University, Atlanta, Georgia 30314, USA*
[5]*School of Physics and Center for Relativistic Astrophysics, Georgia Institute of Technology, Atlanta, Georgia 30332, USA*
[6]*Department of Physics, Southern University, Baton Rouge, Louisiana 70813, USA*
[7]*Department of Physics, University of California, Berkeley, California 94720, USA*
[8]*Lawrence Berkeley National Laboratory, Berkeley, California 94720, USA*
[9]*Institut für Physik, Humboldt-Universität zu Berlin, D-12489 Berlin, Germany*
[10]*Université Libre de Bruxelles, Science Faculty CP230, B-1050 Brussels, Belgium*
[11]*Vrije Universiteit Brussel, Dienst ELEM, B-1050 Brussels, Belgium*
[12]*Department of Physics, Chiba University, Chiba 263-8522 Japan*
[13]*Department of Physics and Astronomy, University of Canterbury, Private Bag 4800, Christchurch, New Zealand*
[14]*Department of Physics, University of Maryland, College Park, Maryland 20742, USA*
[15]*Department of Physics and Center for Cosmology and Astro-Particle Physics, The Ohio State University, 191 W. Woodruff Avenue, Columbus, Ohio 43210, USA*
[16]*Department of Physics, Universität Dortmund, D-44221 Dortmund, Germany*

[17]*Department of Subatomic and Radiation Physics, University of Gent, B-9000 Gent, Belgium*
[18]*Max-Planck-Institut für Kernphysik, D-69177 Heidelberg, Germany*
[19]*Department of Physics and Astronomy, University of California, Irvine, California 92697, USA*
[20]*Laboratory for High Energy Physics, École Polytechnique Fédérale, CH-1015 Lausanne, Switzerland*
[21]*Department of Physics and Astronomy, University of Kansas, Lawrence, Kansas 66045, USA*
[22]*Department of Astronomy, University of Wisconsin, Madison, Wisconsin 53706, USA*
[23]*Department of Physics, University of Wisconsin, Madison, Wisconsin 53706, USA*
[24]*Institute of Physics, University of Mainz, Staudinger Weg 7, D-55099 Mainz, Germany*
[25]*University of Mons-Hainaut, 7000 Mons, Belgium*
[26]*Bartol Research Institute and Department of Physics and Astronomy, University of Delaware, Newark, Delaware 19716, USA*
[27]*Department of Physics, University of Oxford, 1 Keble Road, Oxford OX1 3NP, United Kingdom*
[28]*Department of Physics, University of Wisconsin, River Falls, Wisconsin 54022, USA*
[29]*Department of Physics, Stockholm University, SE-10691 Stockholm, Sweden*
[30]*Department of Astronomy and Astrophysics, Pennsylvania State University, University Park, Pennsylvania 16802, USA*
[31]*Department of Physics, Pennsylvania State University, University Park, Pennsylvania 16802, USA*
[32]*Division of High Energy Physics, Uppsala University, S-75121 Uppsala, Sweden*
[33]*Department of Physics and Astronomy, Utrecht University/SRON, NL-3584 CC Utrecht, The Netherlands*
[34]*Department of Physics, University of Wuppertal, D-42119 Wuppertal, Germany*
[35]*DESY, D-15735 Zeuthen, Germany*

(Received 18 August 2008; revised manuscript received 3 March 2009; published 18 March 2009)

We present a search for point sources of high energy neutrinos using 3.8 yr of data recorded by AMANDA-II during 2000–2006. After reconstructing muon tracks and applying selection criteria designed to optimally retain neutrino-induced events originating in the northern sky, we arrive at a sample of 6595 candidate events, predominantly from atmospheric neutrinos with primary energy 100 GeV to 8 TeV. Our search of this sample reveals no indications of a neutrino point source. We place the most stringent limits to date on E^{-2} neutrino fluxes from points in the northern sky, with an average upper limit of $E^2\Phi_{\nu_\mu+\nu_\tau} \leq 5.2 \times 10^{-11}$ TeV cm^{-2} s^{-1} on the sum of ν_μ and ν_τ fluxes, assumed equal, over the energy range from 1.9 TeV to 2.5 PeV.

DOI: 10.1103/PhysRevD.79.062001 PACS numbers: 95.85.Ry, 98.70.Sa

I. INTRODUCTION

Detecting extraterrestrial sources of high energy ($>$ TeV) neutrinos is a long-standing goal of astrophysics. Neutrinos are neither deflected by magnetic fields nor significantly attenuated by matter and radiation en route to Earth, thus neutrino astronomy offers an undistorted view deep into the high energy universe. Particularly, neutrinos offer an opportunity to probe the sources of high energy cosmic rays, which remain unknown. Potential cosmic ray sources include galactic microquasars and supernova remnants as well as extragalactic sources such as active galactic nuclei and gamma ray bursts. These objects are thought to accelerate protons and nuclei in shock fronts via the Fermi mechanism [1], resulting in power law energy spectra E^α, with $\alpha \sim -2$. A fraction of the energized particles interact with local matter and radiation, producing pions. The neutral pions decay into high energy photons, and the charged pions ultimately produce neutrinos with a flavor ratio ν_e:ν_μ:$\nu_\tau \sim 1$:2:0, mixing to approximately 1:1:1 at Earth because of vacuum flavor oscillations. Observations of TeV gamma rays [2–4] hint at possible cosmic ray source locations but currently cannot separate neutral pion decay spectra from inverse Compton emission. The Auger Collaboration has reported a correlation of arrival directions of the highest energy cosmic rays with active galactic nuclei [5]; however, a similar correlation has not been observed by HiRes [6]. Identification of a high energy neutrino point source would provide an unambiguous signature of energetic hadrons and cosmic ray acceleration. Neutrino flux predictions exist for many potential sources [7–12], but no high energy neutrino point source has yet been identified [13–15].

The search for high energy neutrino point sources is a major objective of the antarctic muon and neutrino detector array (AMANDA). High energy leptons are produced in the Earth by charged-current neutrino interactions. In transparent matter, a cone of Cherenkov photons propagates from the lepton track according to the optical properties of the medium. AMANDA-II is an optical Cherenkov detector consisting of 677 optical modules

*Corresponding author; jbraun@icecube.wisc.edu
†Associated with Universität Erlangen-Nürnberg, Physikalisches Institut, D-91058, Erlangen, Germany.
‡On leave of absence from Università di Bari, Dipartimento di Fisica, I-70126, Bari, Italy.
§Affiliated with School of Pure and Applied Natural Sciences, Kalmar University, S-39182 Kalmar, Sweden.

arranged in 19 strings frozen ~1500 to ~2000 m deep in the ice sheet at the geographic south pole. Approximately 540 modules in the core of the array showing stable performance are used in this search. Each module contains a 20 cm diameter photomultiplier tube (PMT) optically coupled to an outer glass high-pressure sphere. PMT pulses are propagated to surface electronics, and, when the trigger threshold of 24 discriminator crossings ("hits") within 2.5 μs is satisfied, the pulse leading edge times are recorded. The leading edge times along with known detector geometry and optical properties of south pole ice [16] allow reconstruction of tracks passing through the detector [17]. High energy electrons produce short electromagnetic cascades with little directional information of the primary neutrino. Muons produced in the ice and bedrock, on the other hand, propagate up to several kilometers to the detector and their tracks are reconstructed with 1.5°–2.5° median accuracy depending on energy and zenith angle. Tau leptons decay rapidly and produce tracks too short for reconstruction below ~PeV energies. Tau decay, however, contributes high energy muons with a branching ratio of 17.7% [13,18], and these muon tracks can be reconstructed. We thus search for upward propagating muons produced in the Earth by ν_μ ($\bar{\nu}_\mu$) and ν_τ ($\bar{\nu}_\tau$) fluxes following roughly an E^{-2} energy spectrum. While downward neutrino-induced muons also trigger the detector, such events are difficult to distinguish from downward muons produced by cosmic ray air showers. Located at the south pole, AMANDA-II is thus most sensitive to neutrino fluxes from the northern sky. Air showers also produce neutrinos, and this atmospheric neutrino flux [19,20] is the main background for our search.

Here we present the results of a search for astrophysical point sources of high energy neutrinos using 3.8 yr of data recorded by AMANDA-II during 2000–2006, extending the previous five-year analysis [13] with data from the final two years of stand-alone operation and improving our sensitivity by a factor of ~2. We report flux limits for a catalog of 26 selected source candidates along with results of a search for neutrino sources over the entire northern sky. Additionally, we report results from a search for neutrino emission from gamma ray sources identified by Milagro [2] and a search for event angular correlations. In all cases, we observe no indications of an astrophysical neutrino point source.

II. DATA SELECTION

As illustrated in Fig. 1, AMANDA-II records $O(10^9)$ events per year from downward propagating muons produced by cosmic ray air showers, $O(10^3)$ events per year from atmospheric neutrinos, and $O(10)$ high quality events per year from astrophysical E^{-2} neutrino fluxes given current limits [21]. We attempt to isolate these neutrino events from the downward muon background in a computationally efficient manner. We exclude data taken during periods of detector instability and significant maintenance, which include the austral summer (1 November through 15 February). After accounting for dead time in data acquisition electronics, nominally ~15% of up time, we have accumulated 1387 days (3.8 yr) of live time with 1.29×10^{10} events during seven years of operation (Table I).

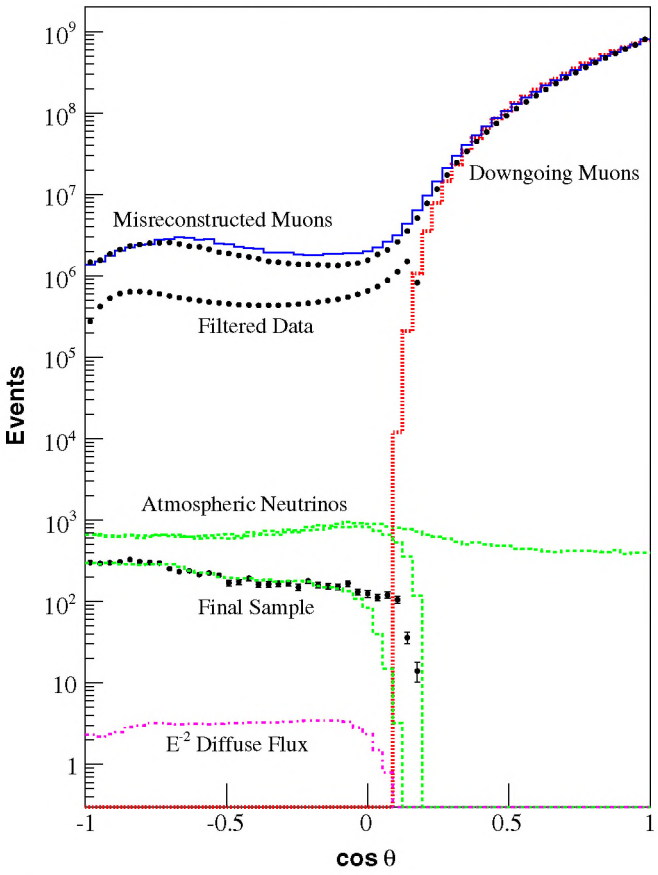

FIG. 1 (color online). Zenith angle (θ) distributions for data and simulation at several reduction levels. Reconstructed (solid line) and true (fine dotted line) zenith angle distributions are shown for CORSIKA [39] cosmic ray muon simulation at retrigger level, and reconstructed zenith angle distributions are shown for atmospheric neutrino simulation (dotted lines) and data (circles) at retrigger level, filter level, and final selection. We also show the reconstructed zenith angle distribution of a diffuse E^{-2} neutrino flux at the current limit [21] using our final selection (dash-dotted line).

Events are first processed to remove hits induced by electrical cross talk, hits from unstable modules, and isolated noise hits [17], and events which no longer pass the trigger criteria are discarded. These retriggered events are then reconstructed with the fast pattern matching algorithms DirectWalk (DW) [17] and JAMS [22] which identify muon tracks within events. For optimal efficiency, our upgoing event selection requires both zenith angles θ_{DW} and θ_{JAMS} greater than 70°–80°.

TABLE I. AMANDA live time and event totals.

Year	Live time	Total events	Filtered events	Final selection
2000	197 d	1.37×10^9	1.63×10^6	596
2001	193 d	2.00×10^9	1.90×10^6	854
2002	204 d	1.91×10^9	2.10×10^6	1009
2003	213 d	1.86×10^9	2.22×10^6	1069
2004	194 d	1.72×10^9	2.09×10^6	998
2005	199 d	2.06×10^9	5.21×10^6	1019
2006	187 d	2.00×10^9	4.89×10^6	1050
Total	1387 d	12.92×10^9	20.04×10^6	6595

Two CPU intensive maximum likelihood reconstructions are applied to events passing the above selection criteria. First, we apply an unbiased likelihood (UL) fit seeded with the DirectWalk and JAMS reconstructed tracks and 30 additional random track directions. The likelihood function [17] parametrizes the probability of observing the obtained geometry and leading edge times of hit modules in terms of track zenith angle, azimuthal angle, and position. The likelihood is maximized with respect to these parameters (in practice, the negative logarithm of the likelihood is numerically minimized), yielding the best fit track zenith and azimuthal angles, and the fit result from the seed yielding the maximum likelihood is chosen as the reconstructed track. A 64 seed Bayesian likelihood (BL) fit is also done, using the downgoing muon zenith angle distribution as a Bayesian prior. With the additional cut $\theta_{\mathrm{UL}} > 80°$, our upgoing event filter reduces the downward muon background by a factor of ~650 relative to trigger level (Table I).

After this cut, $O(10^6)$ misreconstructed downward muon events per year remain, which still outnumber atmospheric neutrinos by roughly 3 orders of magnitude. The vast majority of these events are removed by the following four topological parameters, shown in Fig. 2:

(i) The likelihood ratio of the UL and BL fits. Downgoing muon background events misreconstructed as upgoing by the UL fit typically are also fit well with the downward biased BL reconstruction, whereas true upgoing events are not. Therefore, the UL/BL likelihood ratio tends to be higher for upgoing events.

(ii) The angular uncertainty of the UL fit, described further in Sec. III. Misreconstructed events generally have large angular uncertainty.

(iii) The *smoothness*, or homogeneity of the hit distribution along the UL track [17]. High quality events contain photon hits along the entire length of the track and have smoothness values near zero, whereas hits from misreconstructed events tend to distribute near the beginning or end of the track and have smoothness values near $+1$ and -1, respectively.

(iv) The UL track *direct length*, obtained by projecting *direct hits* backward to the UL track at the Cherenkov angle and taking the distance along the track between the first and last. We select direct hits, compatible with relatively unscattered photons and arriving on time with the Cherenkov cone, using the time window $-15\ \mathrm{ns} < t - t_{\mathrm{ch}} < 25\ \mathrm{ns}$ [17]. Hits from misreconstructed events rarely follow the muon-Cherenkov timing pattern over significant distances, resulting in short lengths.

For the zenith angle region $91.5° < \theta < 180°$ we use the following zenith angle dependent cuts, optimized to yield maximum sensitivity [23]:

$$\log(\mathrm{UL}/\mathrm{BL}) > 34 - 25 \cdot \Phi(\cos\theta + 0.15)$$
$$\sigma_i < 3.2 - 4 \cdot \Phi(-\cos\theta - 0.75)$$
$$|\mathrm{smoothness}| < 0.36.$$

Here $\Phi(x) = x$ for positive x, and $\Phi(x) = 0$ for $x < 0$. We use a support vector machine (SVM) [24] trained on the four parameters to improve event selection in the near-horizontal region $80° < \theta < 91.5°$. Events with SVM quality of zero or less are consistent with misreconstructed muon background, while events with larger values of SVM quality are increasingly consistent with quality muons. We apply the cut:

$$\mathrm{SVM\ quality} > 1 - 12 \cdot \Phi(\cos\theta - 0.023).$$

Application of these quality cuts yields 6595 neutrino candidate events [25] (Fig. 3).

Simulations of two atmospheric neutrino flux models [19,20], with events generated by ANIS [26] and resultant muons propagated to the detector with MMC [27], both agree with data in track quality parameter distributions and zenith angle (Fig. 2) within the ~30% uncertainty in these flux predictions. Application of the filter selection and final quality cuts to this simulation yield an atmospheric neutrino efficiency of 30% relative to the retrigger level for $\theta > 90°$. The contribution of misreconstructed downward muons has been estimated by subtracting the simulated atmospheric neutrino rate, after renormalizing it for a more stringent selection yielding a nearly pure neutrino sample. The muon contamination has been found to be less than 5% for $\theta > 95°$ (declination $\delta > 5°$), but the contamination is more significant near the equator and dominates events in the southern sky. A parallel analysis of these atmospheric neutrino events has revealed no evidence of new physics such as violation of Lorentz invariance and quantum decoherence [28]. We simulate ν_μ and ν_τ events from 10 GeV to 100 PeV with an identical software chain, and this simulation is used to calculate the neutrino effective area, shown in Fig. 4, and flux limits

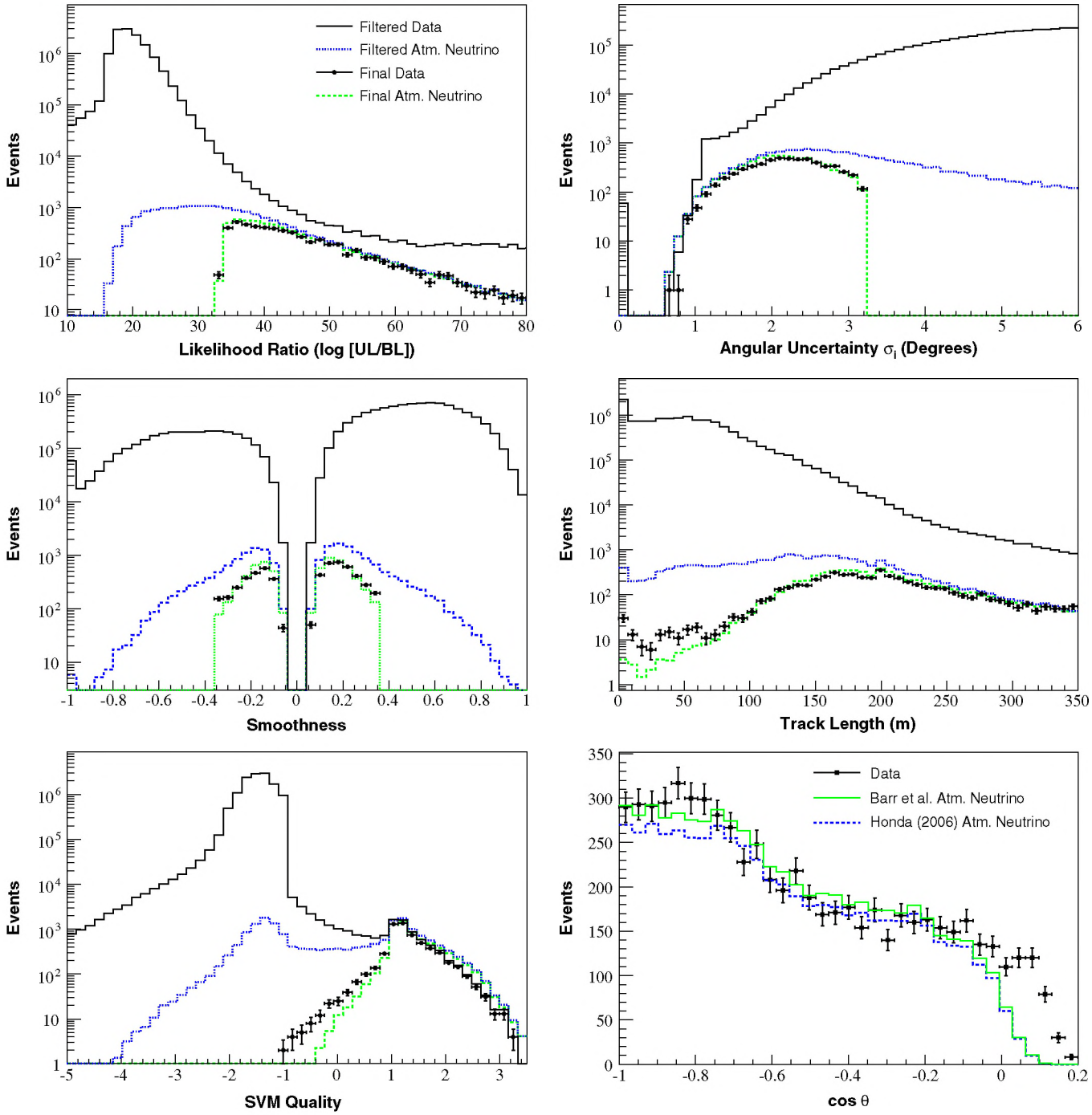

FIG. 2 (color online). Distributions of data and atmospheric neutrinos at filter level and final selection level for several parameters and zenith angles $\theta > 95°$ (top and left panels), and zenith angle distribution for the selected 6595 neutrino candidate events compared with model predictions [19,20] for atmospheric neutrinos (bottom right panel).

for neutrino sources with E^{-2} energy spectra. The central 90% of such signal events fall within the energy range 1.9 TeV to 2.5 PeV. The median accuracy of the UL fit when applied to simulated events following an E^{-2} energy spectrum is 1.5°–2.5°, shown in Fig. 5. The absolute pointing accuracy of AMANDA has been confirmed by observing downgoing muon events coincident with well-reconstructed air showers recorded by SPASE [17] and events coincident with IceCube.

III. SEARCH METHOD

The remaining background, mostly atmospheric neutrinos, is difficult to reduce further without significantly decreasing signal efficiency. Neutrinos from E^{-2} sources

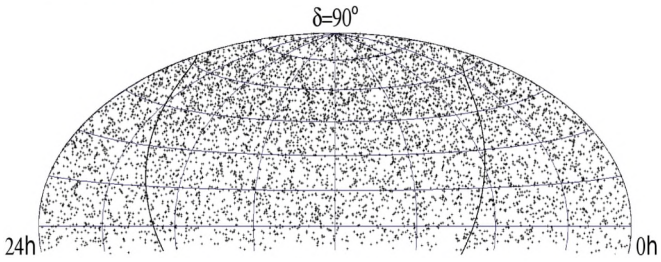

FIG. 3 (color online). Equatorial sky map of 6595 events recorded by AMANDA-II from 2000–2006. A table of the events is available [25].

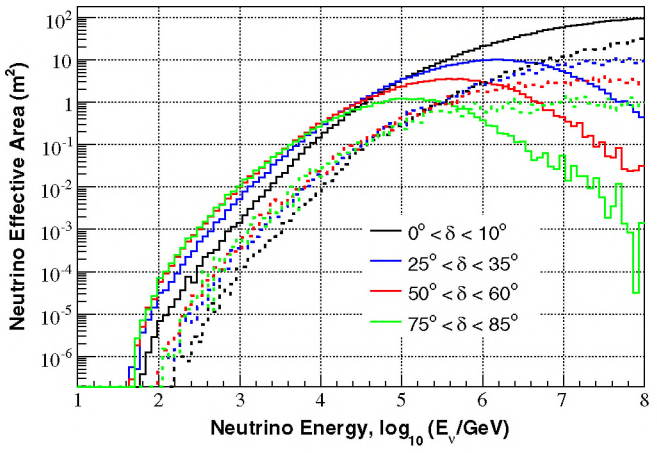

FIG. 4 (color online). Effective area for averaged ν_μ and $\bar{\nu}_\mu$ (solid lines) and averaged ν_τ and $\bar{\nu}_\tau$ (dashed lines) neutrino fluxes for several declination ranges.

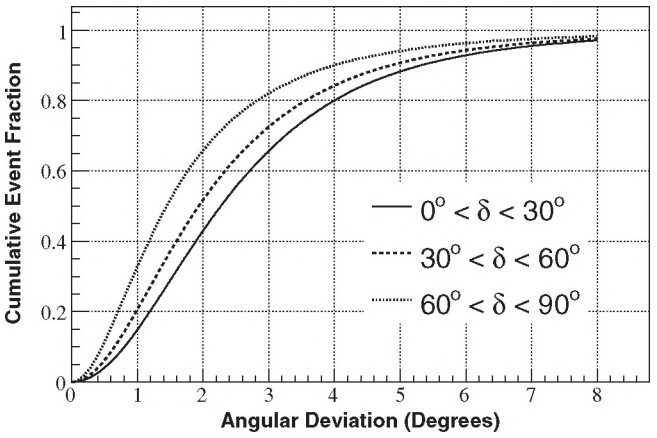

FIG. 5. Angular deviation between neutrino and UL fit track for simulated E^{-2} muon neutrino events from several declination ranges.

are typically more energetic than atmospheric neutrinos (Fig. 6), which follow a steeper $\sim E^{-3.7}$ energy spectrum. We search our sample of 6595 events for excesses above the atmospheric neutrino background both in direction and event energy using an unbinned maximum likelihood

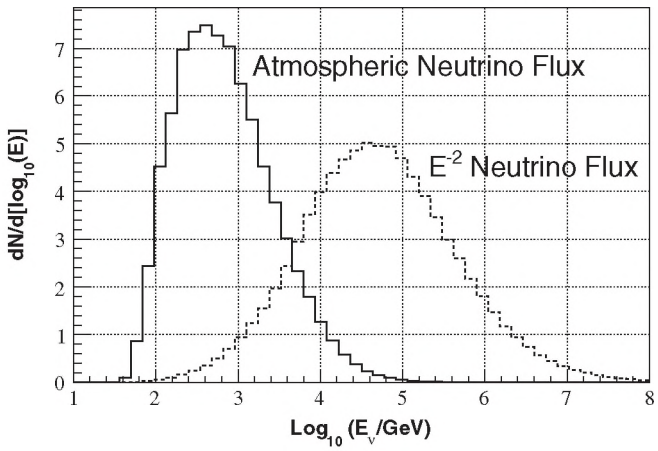

FIG. 6. Energy distribution of events passing selection criteria for simulated atmospheric neutrino background [19] in a 3.5° bin and an E^{-2} point source with flux $\Phi_{\nu_\mu+\nu_\tau} = 10^{-10}$ TeV cm^{-2} s^{-1}. Such a source would be detected at 5σ in approximately 40% of trials.

search method [29], providing direction and energy discrimination on an event-by-event basis by incorporating an event angular resolution estimate and energy estimate.

A. Event angular uncertainty estimation

Our ability to reconstruct muon tracks in AMANDA partially depends on event topology. A muon track passing through a larger portion of the detector or giving hits in a larger number of modules should, on average, reconstruct with better angular resolution due to a longer lever arm or larger number of measurement points, respectively. We therefore estimate the resolution of each UL track by evaluating the likelihood space near the maximum [30]. As the track zenith angle and azimuthal angle coordinates (θ, ϕ) move away from the best fit track values $(\hat{\theta}, \hat{\phi})$, the quantity $\log\mathcal{L}$ decreases parabolically from its maximum. The likelihood ratio $-2 \cdot \log(\frac{\mathcal{L}(\theta,\phi)}{\mathcal{L}(\hat{\theta},\hat{\phi})})$ is evaluated on a grid of zenith and azimuthal angles near the best track, and the resulting values are fit to a paraboloid with the form

$$-2 \cdot \log\left(\frac{\mathcal{L}(\theta, \phi)}{\mathcal{L}(\hat{\theta}, \hat{\phi})}\right) = \frac{x^2}{\sigma_x^2} + \frac{y^2}{\sigma_y^2}, \tag{1}$$

where the x and y axes are fit and do not necessarily correspond to zenith and azimuthal angles. The two errors σ_x and σ_y are then geometrically averaged into a single, circular error σ_i. The paraboloid fit is thus a convenient approximation of the likelihood space, reducing the complex map of $-2 \cdot \log(\frac{\mathcal{L}(\theta,\phi)}{\mathcal{L}(\hat{\theta},\hat{\phi})})$ into just σ_i. The corresponding spatial probability density estimate at an angular distance Ψ is then

$$P(\Psi_i) = \frac{e^{-(\Psi^2/2\sigma_i^2)}}{2\pi\sigma_i^2}. \tag{2}$$

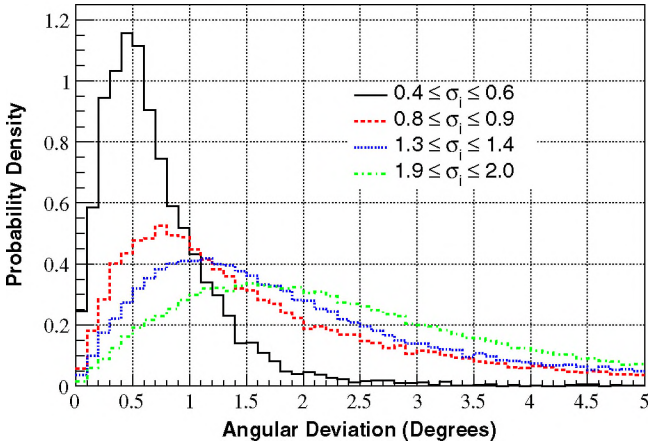

FIG. 7 (color online). Distributions of angular deviation between true and reconstructed tracks for simulated neutrino events over several ranges of estimated angular uncertainty.

Distributions of the angular deviation between true and reconstructed neutrino tracks for several ranges of estimated angular uncertainty (Fig. 7) show the correlation between estimated angular uncertainty and track reconstruction error.

B. Event energy estimation

The amount of light deposited in the detector depends strongly on muon energy above ~1 TeV, and thus the number of hit modules ($N_{\rm ch}$) provides an approximate measure of event energy. Distributions of muon energy for several ranges of $N_{\rm ch}$ (Fig. 8) show the performance of $N_{\rm ch}$ as a muon energy estimator, with a 1σ uncertainty in $\log_{10}(E_\mu/\mathrm{GeV})$ of 0.65. Rather than measure event absolute energy, it is more relevant for a neutrino search to assess the compatibility of an event with expected astrophysical neutrino spectra, assumed to follow a power law. From simulations, we tabulate $N_{\rm ch}$ probabilities for spectral indices $1 \le \gamma \le 4$ in bins of 0.01 and for atmospheric neutrinos [19], shown in Fig. 8. This $N_{\rm ch}$ probability table yields the probability of observing a given $N_{\rm ch}$ value from a source with a power law energy spectrum relative to observing the value from background atmospheric neutrinos.

C. Maximum likelihood method

For a source with position $\vec{x}_s$, giving n_s events against a background of $N - n_s$ events, the probability density is

$$\frac{n_s}{N}\mathcal{S} + \left(1 - \frac{n_s}{N}\right)\mathcal{B}, \tag{3}$$

where $\mathcal{S}$ and $\mathcal{B}$ are the probability densities for signal and background, respectively. The likelihood function is

$$\mathcal{L} = \prod_{i=1}^{N}\left(\frac{n_s}{N}\mathcal{S}_i + \left(1 - \frac{n_s}{N}\right)\mathcal{B}_i\right), \tag{4}$$

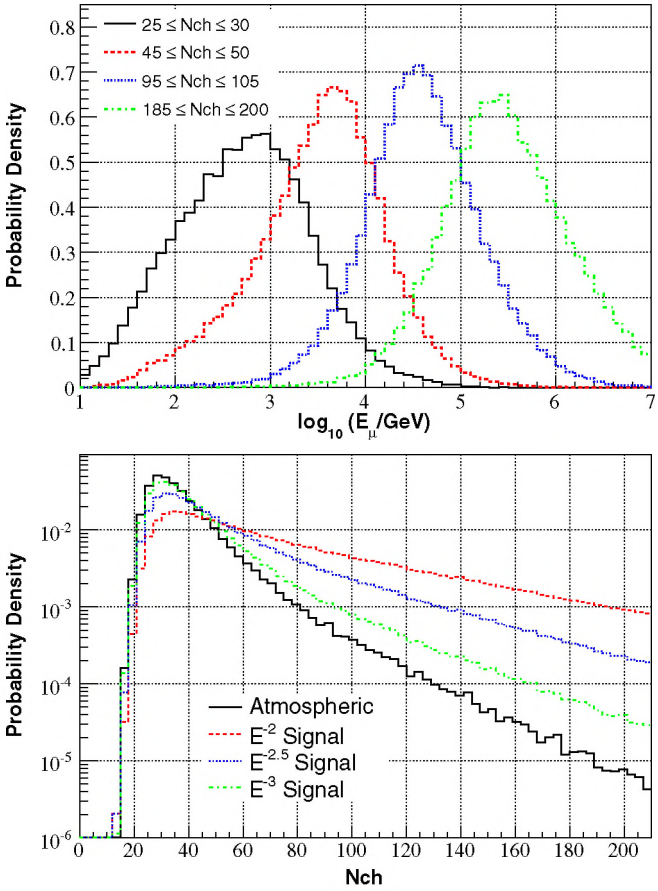

FIG. 8 (color online). Muon energy distributions for four ranges of $N_{\rm ch}$ (top panel), and simulated $N_{\rm ch}$ distributions for atmospheric neutrinos [19] and E^{-2}, $E^{-2.5}$, and E^{-3} power law neutrino spectra (bottom panel).

where i runs over the selected events. Events are assumed to have an angular error distributed according to a Gaussian given by the event angular uncertainty σ_i, and signal events are assumed to follow a power law energy spectrum with spectral index γ. The signal probability density for an event at $\vec{x}_i$ is

$$\mathcal{S}_i = \frac{1}{2\pi\sigma_i^2} e^{-(|\vec{x}_i - \vec{x}_s|^2/2\sigma_i^2)} P(N_{{\rm ch},i}|\gamma), \tag{5}$$

where $|\vec{x}_i - \vec{x}_s|$ is the angular distance between the event and assumed source position. In practice, we only include events with declinations $\pm 8°$ of the source declination since events outside this band have extremely low signal probabilities, and we set N to be the number of events in this declination band. The background probability over this band is roughly constant and given by

$$\mathcal{B}_i = \frac{P(N_{{\rm ch},i}|\phi_{\rm atm})}{\Omega_{\rm band}}. \tag{6}$$

The likelihood $\mathcal{L}$ is maximized (again, $-\log\mathcal{L}$ is numeri-

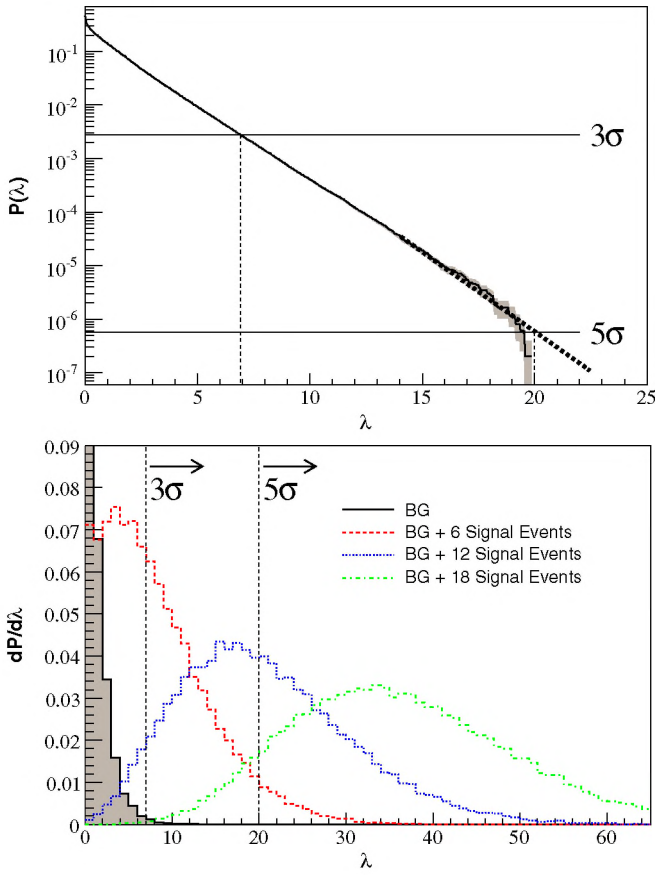

FIG. 9 (color online). Integral distribution of the test statistic for background at $\delta = 42.5°$ with 3σ and 5σ thresholds indicated and statistical uncertainty shaded in gray (top panel), and distribution of the test statistic for background and 6, 12, and 18 added E^{-2} signal events at $\delta = 42.5°$ (bottom panel).

cally minimized) with respect to n_s and γ, resulting in best fit signal strength $\hat{n}_s$ and spectral index $\hat{\gamma}$. The data are then compared to the null, background-only hypothesis ($n_s = 0$) to determine relative compatibility. We use as our test statistic

$$\lambda = -2 \cdot \log\left(\frac{\mathcal{L}(n_s = 0)}{\mathcal{L}(\hat{n}_s, \hat{\gamma})}\right). \quad (7)$$

Larger values of λ reject the null hypothesis with increasing confidence, shown in Fig. 9. The significance of a particular value of λ is determined by comparing the obtained value to the distribution of test statistic values at the same location from data randomized in right ascension, and we denote as p the fraction of randomized data sets with higher test statistic values. This method, by using unbinned event-by-event energy and directional discrimination, improves the sensitivity to E^{-2} neutrino fluxes by more than 30% relative to the previous method [31] using angular bins.

TABLE II. Systematic errors in event rate expectations for point sources with E^{-2} energy spectra.

Source	Magnitude
Neutrino cross section and rock density	$\pm 8\%$
Optical module sensitivity	$^{+2}_{-9}\,\%$
Photon propagation	$\pm 5\%$
Event selection bias	$^{+0}_{-7}\,\%$
Event reconstruction bias	$^{+0}_{-7}\,\%$
Other known sources	$<4\%$
Total	$^{+10}_{-17}\,\%$

IV. SEARCH FOR POINT SOURCES IN THE NORTHERN SKY

We first apply the search to a predefined list of 26 energetic galactic and extragalactic objects, including many TeV gamma ray sources. For each source location, we compute the value of the unbinned search test statistic λ. Flux upper limits are computed from the test statistic using Feldman-Cousins unified ordering [32]. Systematic uncertainties are incorporated into the limit calculation using the method of Conrad *et al.* [33] as modified by Hill [34]. We estimate the total systematic uncertainty in our event rate expectations for E^{-2} fluxes to be 17%, summarized in Table II. Significant contributions include the absolute sensitivity of optical modules (9%), neutrino interaction cross section (8%), bias in event selection between data and simulation (7%), and photon propagation in the ice (5%), determined by detailed detector studies presented in [13]. Additionally, we evaluate bias in reconstruction accuracy by comparing distributions of event angular resolution estimates (σ_i) with those from point source simulations. We find the angular resolution estimates in simulation are typically 8% smaller, and adjusting our simulated point spread by this factor results in flux limits 7% higher. Other known sources of systematic uncertainty, including uncertainties in optical module timing resolution and the search method, total less than 4%. Limits on $\nu_\mu + \nu_\tau$ fluxes at 90% confidence level and chance probabilities (p) are shown in Table III. Limits on ν_μ fluxes alone correspond to half these values. The highest significance is found for Geminga with $p = 0.0086$. The probability of obtaining $p \leq 0.0086$ by chance for at least one of 26 sources is 20% and is therefore not significant.

We then apply the search to declinations $-5° < \delta < 83°$ on a $0.25° \times 0.25°$ grid. The region above declination $83°$ is left to a dedicated search for weakly interacting massive particle (WIMP) annihilation at the center of the Earth [35]. For each grid point, we similarly compute a flux limit and significance (Fig. 10). We find a maximum pretrial significance of $p = 7.4 \times 10^{-4}$ at $\delta = 54°$, $\alpha = 11.4h$. We account for the trial factor associated with the all sky search by comparing the maximum pretrial signifi-

TABLE III. Flux upper limits for 26 neutrino source candidates: Source declination, right ascension, 90% confidence level upper limits for $\nu_\mu + \nu_\tau$ fluxes with E^{-2} spectra ($E^2\Phi_{\nu_\mu+\nu_\tau} \leq \Phi_{90} \times 10^{-11}$ TeV cm^{-2} s^{-1}) over the energy range 1.9 TeV to 2.5 PeV, pretrials significance, median angular resolution of primary neutrino, and number of events inside a cone centered on the source location with radius equal to the median point spread. Since event energy is an important factor in the analysis, the number of nearby events does not directly correlate with pretrials significance.

Candidate	$\delta(^\circ)$	$\alpha(h)$	Φ_{90}	p	$\Psi(^\circ)$	N
3C 273	2.05	12.49	8.71	0.086	2.1	3
SS 433	4.98	19.19	3.21	0.64	2.2	1
GRS 1915 + 105	10.95	19.25	7.76	0.11	2.3	8
M87	12.39	12.51	4.49	0.43	2.3	3
PKS 0528 + 134	13.53	5.52	3.26	0.64	2.3	0
3C 454.3	16.15	22.90	2.58	0.73	2.3	5
Geminga	17.77	6.57	12.77	0.0086	2.3	2
Crab Nebula	22.01	5.58	9.27	0.10	2.3	7
GRO J0422 + 32	32.91	4.36	2.75	0.76	2.2	3
Cyg X-1	35.20	19.97	4.00	0.57	2.1	3
MGRO J2019 + 37	36.83	20.32	9.67	0.077	2.1	7
4C 38.41	38.14	16.59	2.20	0.85	2.1	4
Mrk 421	38.21	11.07	2.54	0.82	2.1	3
Mrk 501	39.76	16.90	7.28	0.22	2.0	6
Cyg A	40.73	19.99	9.24	0.095	2.0	3
Cyg X-3	40.96	20.54	6.59	0.29	2.0	8
Cyg OB2	41.32	20.55	6.39	0.30	2.0	8
NGC 1275	41.51	3.33	4.50	0.47	2.0	4
BL Lac	42.28	22.05	5.13	0.38	2.0	2
H 1426 + 428	42.68	14.48	5.68	0.36	2.0	3
3C66A	43.04	2.38	8.06	0.18	2.0	6
XTE J1118 + 480	48.04	11.30	5.17	0.50	1.8	3
1ES 2344 + 514	51.71	23.78	5.74	0.44	1.7	2
Cas A	58.82	23.39	3.83	0.67	1.6	2
LS I +61 303	61.23	2.68	14.74	0.034	1.5	5
1ES 1959 + 650	65.15	20.00	6.76	0.44	1.5	5

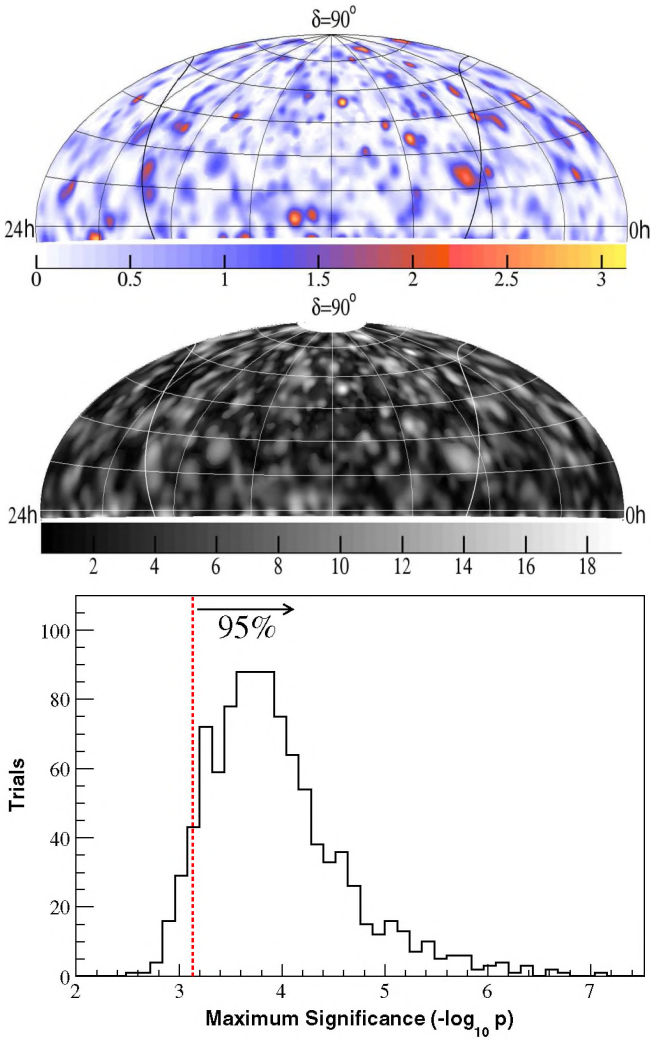

FIG. 10 (color online). Sky map of significances ($-\log_{10}p$) obtained in the full-sky search excluding trial factors (top panel), sky map of $\nu_\mu + \nu_\tau$ 90% confidence level flux upper limits for an E^{-2} energy spectrum (10^{-11} TeV cm^{-2} s^{-1}) over the energy range 1.9 TeV to 2.5 PeV (middle panel), and the distribution of maximum significances for 1000 randomized sky maps, with the obtained significance $p = 7.4 \times 10^{-4}$ dotted (bottom panel).

cance to the distribution of maximum pretrial significances obtained from sky maps randomized in right ascension. We find 95% of sky maps randomized in right ascension have a maximum significance of at least $p = 7.4 \times 10^{-4}$ (Fig. 10). Sensitivity and flux limits are summarized in Fig. 11.

In the northern sky, the galactic TeV gamma ray sources observed by Milagro [2] are promising candidates for observation with neutrino telescopes [11,12]. We improve our ability to detect a weak signal from this class of objects by $\sim\sqrt{N}$ by combining N sources of similar strength, with less improvement if one source is much stronger than average. We include five of eight sources and source candidates observed by Milagro with significance above 5σ before considering trial factors, including four regions near Cygnus and one near the equator. We add a hot spot near $\delta = 1^\circ$, $\alpha = 19h$ [36], which may be associated with a large neutrino flux if confirmed as a source [11]. We exclude the three regions with pulsar-wind nebula counterparts, C3, C4, and the Crab Nebula, which are considered weaker candidates for significant hadron acceleration [11]. We adapt a method developed by HiRes [37] to perform our maximum likelihood search simultaneously for all six source locations, resulting in the slightly modified likelihood function

$$\mathcal{L} = \prod_{i=1}^{N}\left(\frac{1}{6}\cdot\frac{n_s}{N}\sum_{j=1}^{6}\mathcal{S}_i^j + \left(1-\frac{n_s}{N}\right)\mathcal{B}_i\right), \qquad (8)$$

where $\mathcal{S}_i^j$ is the signal probability density of the ith event evaluated for the jth source. Significance is again com-

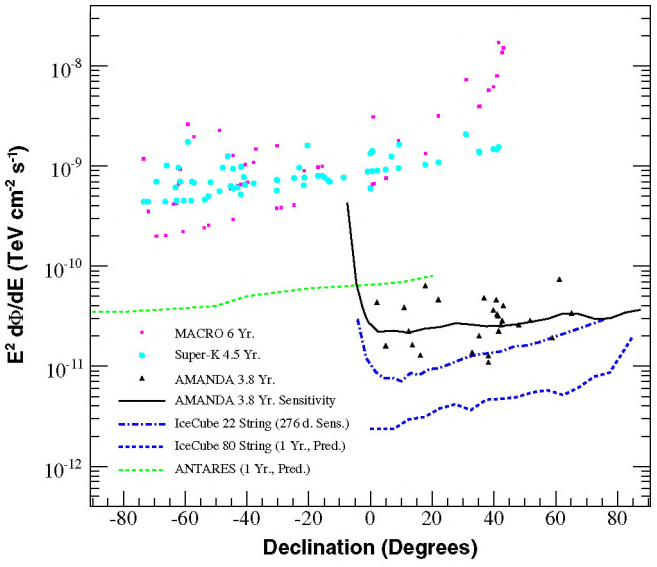

FIG. 11 (color online). Limits on an E^{-2} muon neutrino flux for sources in Table III from this work (triangles), limits from MACRO [14], and Super-K [15], E^{-2} ν_μ sensitivity for this work and the IceCube 22-string analysis, and predicted sensitivity for ANTARES [40] and IceCube. Our $\nu_\mu + \nu_\tau$ limits are divided by 2 for comparison with limits on only ν_μ.

puted by comparing the obtained test statistic value to the distribution obtained from data randomized in right ascension. We observe a small excess with a chance probability of 20%. The 90% confidence level upper limit obtained on the mean ν_μ flux per source is 9.7×10^{-12} TeV cm^{-2} s^{-1}.

Finally, we search for groups of neutrino sources and extended regions of neutrino emission by scanning for correlations of events at all angular distances up to 8°. We perform the search over a range of energy thresholds, using the number of modules hit as an energy parameter. For each threshold in angular distance and number of modules hit, we count the number of event pairs in the data and compare with the distribution of pairs from data randomized in right ascension to compute significance. The highest obtained significance is $p = 0.1$ with a threshold of 146 modules hit and 2.8° angular separation, where we observe two event pairs. The probability of observing this maximum significance by chance is 99%. Since four separate analyses are performed on the data, the probability of obtaining at least one significant result is increased. The most significant result obtained has a chance probability of 20%, and the binomial probability of obtaining this chance fluctuation in at least one of the four analyses is 59% and not significant.

V. CONCLUSIONS

We have analyzed 3.8 yr of AMANDA-II data and found no evidence of high energy neutrino point sources. We place the most stringent limits to date on astrophysical point source fluxes. IceCube [38] is a next-generation neutrino telescope at the South Pole scheduled for completion in 2011 with 80 60-module strings instrumenting $\sim$1 km^3 of ice. Analysis of data recorded during 2007–2008 with the first 22 strings has improved the AMANDA-II sensitivity by a factor of 2. Currently 59 strings are operating, and with continued construction IceCube will achieve an angular resolution of better than 1° and an order of magnitude improvement over the AMANDA-II sensitivity within a few years.

ACKNOWLEDGMENTS

We acknowledge the support from the following agencies: U.S. National Science Foundation–Office of Polar Programs, U.S. National Science Foundation–Physics Division, University of Wisconsin Alumni Research Foundation, U.S. Department of Energy and National Energy Research Scientific Computing Center, Louisiana Optical Network Initiative (LONI) grid computing resources, Swedish Research Council, Swedish Polar Research Secretariat, Knut and Alice Wallenberg Foundation (Sweden), German Ministry for Education and Research (BMBF), Deutsche Forschungsgemeinschaft (DFG), (Germany), Fund for Scientific Research (FNRS-FWO), Flanders Institute to encourage scientific and technological research in industry (IWT), Belgian Federal Science Policy Office (Belspo), and the Netherlands Organisation for Scientific Research (NWO); M. Ribordy acknowledges the support of the SNF (Switzerland); A. Kappes and A. Groß acknowledge support by the EU Marie Curie OIF Program; M. Stamatikos is supported by NPP at NASA–GSFC administered by ORAU.

[1] E. Fermi, Phys. Rev. **75**, 1169 (1949).
[2] A. Abdo *et al.*, Astrophys. J. Lett. **664**, L91 (2007).
[3] F. Aharonian *et al.*, Astrophys. J. **636**, 777 (2006).
[4] J. Albert *et al.*, Science **312**, 1771 (2006).
[5] J. Abraham *et al.*, Science **318**, 938 (2007).
[6] R. Abbasi *et al.*, Astropart. Phys. **30**, 175 (2008).
[7] F. Aharonian *et al.*, J. Phys. Conf. Ser. **39**, 408 (2006).
[8] D. Torres and F. Halzen, Astropart. Phys. **27**, 500 (2007).
[9] W. Bednarek *et al.*, New Astron. Rev. **49**, 1 (2005).
[10] F. W. Stecker, Phys. Rev. D **72**, 107301 (2005).
[11] F. Halzen, A. Kappes, and A. OMurchadha, Phys. Rev. D **78**, 063004 (2008).

[12] J. F. Beacom and M. D. Kistler, Phys. Rev. D **75**, 083001 (2007).
[13] A. Achterberg *et al.*, Phys. Rev. D **75**, 102001 (2007).
[14] M. Ambrosio *et al.*, Astrophys. J. **546**, 1038 (2001).
[15] S. Desai *et al.*, Astropart. Phys. **29**, 42 (2008).
[16] M. Ackermann *et al.*, J. Geophys. Res. **111**, D13203 (2006).
[17] J. Ahrens *et al.*, Nucl. Instrum. Methods Phys. Res., Sect. A **524**, 169 (2004).
[18] S. Eidelman *et al.*, Phys. Lett. B **592**, 1 (2004).
[19] G. Barr *et al.*, Phys. Rev. D **70**, 023006 (2004).
[20] M. Honda *et al.*, Phys. Rev. D **75**, 043006 (2007).
[21] A. Achterberg *et al.*, Phys. Rev. D **76**, 042008 (2007).
[22] M. Ackermann, Ph.D. thesis, Humboldt-Universität, Berlin, 2006.
[23] G. C. Hill and K. Rawlins, Astropart. Phys. **19**, 393 (2003).
[24] T. Joachims, in *Advances in Kernel Methods—Support Vector Learning*, edited by B. Schölkopf, C. Burges, and A. Smola (MIT Press, Cambridge, MA, 1999), p. 169.
[25] A table of the AMANDA final event sample is available at http://www.icecube.wisc.edu/science/data.
[26] A. Gazizov and M. Kowalski, Comput. Phys. Commun. **172**, 203 (2005).
[27] D. Chirkin and W. Rhode, arXiv:hep-ph/0407075.
[28] R. Abbasi *et al.*, arXiv:0902.0675.
[29] J. Braun *et al.*, Astropart. Phys. **29**, 299 (2008).
[30] T. Neunhöffer, Astropart. Phys. **25**, 220 (2006).
[31] M. Ackermann *et al.*, IceCube Collaboration, arXiv:0711.0353.
[32] G. J. Feldman and R. D. Cousins, Phys. Rev. D **57**, 3873 (1998).
[33] J. Conrad *et al.*, Phys. Rev. D **67**, 012002 (2003).
[34] G. C. Hill, Phys. Rev. D **67**, 118101 (2003).
[35] A. Achterberg *et al.*, Astropart. Phys. **26**, 129 (2006).
[36] A. Abdo, Ph.D. thesis, Michigan State University, 2007.
[37] R. Abbasi *et al.*, Astrophys. J. **636**, 680 (2006).
[38] J. Ahrens *et al.*, Astropart. Phys. **20**, 507 (2004).
[39] D. Heck *et al.*, Forschungszentrum Karlsruhe Report No. FZKA 6019, 1998.
[40] J. Aguilar, arXiv:0710.0252.